Journal of Hazardous Materials 178 (2010) 144–151

Contents lists available at ScienceDirect

Journal of Hazardous Materials

journal homepage: www.elsevier.com/locate/jhazmat

Simulation and assessment of SO_2 toxic environment after ignition of uncontrolled sour gas flow of well blowout in hills

Yuan Zhu, Guo-ming Chen*

Department of Safety Engineering, China University of Petroleum, Dongying 257061, China

ARTICLE INFO

Article history:
Received 10 September 2009
Received in revised form 1 January 2010
Accepted 12 January 2010
Available online 18 January 2010

Keywords:
Ignition
Well blowout
Sulfur dioxide
LES
Hill

ABSTRACT

To study the sulfur dioxide (SO_2) toxic environment after the ignition of uncontrolled sour gas flow of well blowout, we propose an integrated model to simulate the accident scenario and assess the consequences of SO_2 poisoning. The accident simulation is carried out based on computational fluid dynamics (CFD), which is composed of well blowout dynamics, combustion of sour gas, and products dispersion. Furthermore, detailed complex terrains are built and boundary layer flows are simulated according to Pasquill stability classes. Then based on the estimated exposure dose derived from the toxic dose–response relationship, quantitative assessment is carried out by using equivalent emergency response planning guideline (ERPG) concentration. In this case study, the contaminated areas are graded into three levels, and the areas, maximal influence distances, and main trajectories are predicted. We show that wind drives the contamination and its distribution to spread downwind, and terrains change the distribution shape through spatial aggregation and obstacles. As a result, the most dangerous regions are the downwind areas, the foot of the slopes, and depression areas such as valleys. These cause unfavorable influences on emergency response for accident control and public evacuation. In addition, the effectiveness of controlling the number of deaths by employing ignition is verified in theory. Based on the assessment results, we propose some suggestions for risk assessment, emergency response and accident decision making.

1. Introduction

For sour gas well blowout, which is one of the most serious accidents resulting from gas field exploitation, ignition of uncontrolled flow is recommended or constrained by various standards, laws, or directives [1–3]. In China, after the disaster of the '12.23' Kaixian blowout accident in which 243 people died mostly due to a too-long-delayed ignition decision [4], immediate ignition under extreme conditions was emphasized in drilling safety in such gas fields. For example, the new enterprise standard focusing on the highly sour gas field exploitation in the northeast of Sichuan demands that out-of-control well blowouts must be ignited within 5 min [2]. To comply with the supervision requirements, ignition is probably what will be faced in the event of an accidental sour gas well blowout. During the combustion of sour gas, huge amounts of sulfur dioxide (SO_2) which is an irritation of the upper respiratory tract and eyes will be produced and can cause serious injury to people [1]. Consequently, there is a potential threat to the general public surrounding the well of exposure to the toxic environment formed by the dispersed SO_2.

Detailed safety analysis of sour gas well blowout has been carried out because of the serious consequences. Research on the Kaixian disaster, in particular, has extended our knowledge in this field. Li et al. elaborated the basic information of the accident and made a systematical analysis [4]. Wellhead jet dynamics used for further research was modeled according to well-bore inflow [5]. Movement of hydrogen sulfide in complex terrains and its influence have been simulated based on computational fluid dynamics (CFD) and validated by accident investigation [6,7]. However, these works are still lacking in regard to ignition and SO_2 poisoning.

Therefore, analysis of the ignition process and quantitative assessment of the risk of SO_2 are very much needed. In this field, the Energy Resources Conservation Board (ERCB) releases a dedicated software, ERCBH_2S, that includes an assessment model for SO_2. Due to the method of parallel airflow modeling, this model is more suitable for flat terrains [8]. However, as most sour gas fields are in the hill regions of the northeast of Sichuan in China, the effects of complex terrains on gas dispersion should be included. Although much research on the atmospheric flow over hills has been carried out based on field measurement, laboratory experiments, and numerical methods [6,7,9–11], reactive sour gas transportation is not mentioned. In these works, CFD simulation, with the advantages of low cost, high efficiency, and powerful modeling capabilities, has been widely adopted [6,7,10,11]. The results of the comparison

* Corresponding author. Tel.: +86 05468391113; fax: +86 05468393914.
E-mail address: ogsafety@126.com (G.-m. Chen).

0304-3894/$ – see front matter © 2010 Elsevier B.V. All rights reserved.
doi:10.1016/j.jhazmat.2010.01.055

Nomenclature

A	tubing or casing area (m^2)
c	sulfide dioxide concentration (ppm)
C_D	drag coefficient 0.0–1.0
c_{eq}	equivalent ERPG concentration (ppm)
c_k, c_{k+1}	sulfide dioxide concentration at consecutive interpolation point (ppm)
c_p	specific heat capacity at constant pressure (J/kg/K)
C_v	constant 0.5
f	mixture fraction
g	gravitational acceleration (m/s^2)
H	total enthalpy (J/kg)
H_c	mass-average heat of combustion (J/kg)
k_t	turbulent thermal conductivities (W/m/K)
L	toxic dose (ppm^n min)
L_f	length of flame (m)
L_s	subgrid filter length (m)
m_E	wellhead mass flux (kg/s)
n	constant 1.0
$p(f)$	probability density function
P_a	atmospheric pressure (Pa)
P_E	choked pressure (Pa)
Q_{rad}	heat of radiation (J/s)
R_f	radius of flame at distance s_f (m) along center line of flame
S	user-defined source term for species ($kg/m^3/s$)
S_h	user-defined source term for enthalpy ($J/m^3/s$)
S_{rad}	heat of radiation ($J/m^3/s$)
t	time (s)
T	temperature (K)
u	velocity (m/s)
v_1, v_2	wind speed (m/s) at altitude z_1 and z_2 (m)
V	inlet velocity (m/s)
V_E	choked velocity (m/s)
V_f	volume of flame (m^3)
Y	probit
Z	elemental mass fraction

Greek letters

ϕ_i	represents the instantaneous species mass fraction, density (kg/m^3), or temperature (K)
η	fraction of total energy converted to radiation 0.2
μ	molecular viscosity (Pa s)
μ_t	turbulent viscosity (Pa s)
ρ	density (kg/m^3)
ρ_E	inertial exit density (kg/m^3)
σ_t	constant 0.85
τ	time (min)
τ_E	endpoint of exposure time (min)
$\Delta\tau$	time step size (min)

Subscripts

ox	at the oxidizer stream inlet
fuel	at the fuel stream inlet
i, j	spatial coordinates

LES notation

~	LES filtered quantity
–	LES density-weighted filtered quantity

Acronyms

CFD	computational fluid dynamics
DNS	direct numerical simulation
ERCB	Energy Resources Conservation Board
ERPG	emergency response planning guideline
LES	large eddy simulation
RANS	Reynolds averaging Navier–Stokes equation
RFL	rich flammability limit

between CFD prediction and experiments show that this method is quite useful when modeling plume dispersion on complex topography. For reactive pollutant transportation, the CFD method has been applied to simulate the fire-induced plume dispersion in street canyons [12]. As the governing equations are the same for the reactive dispersion, the model used in street canyons could be transferred to complex terrains. And this method has been used by ENI Exploration and Production to do a complete risk analysis of the ignited jet associated with the blowout, in which a series of combustion simulations is carried out and the far-field impact about soot is assessed [13,14].

In order to achieve systemic and comprehensive analysis, CFD is adopted to simulate the accident by using FLUENT software [15]. Then the assessment of toxic environment is made based on predicted concentration and distribution of SO_2.

2. Theoretical model

The accident process is divided into three consecutive stages: wellhead jet, sour gas combustion and products dispersion. As a whole, in order to achieve simulation in a consistent model, the ideal gas law for an incompressible flow is applied and gas density is computed as:

$$\rho = \frac{P_a M}{RT} \tag{1}$$

This is a common assumption in CFD simulation on atmospheric flow [6,7]. For combustion, as far-field assessment on SO_2 is the main concern in this study, the pressure expansion due to combustion is ignored so that the rise of plume is underestimated, which produces more conservative results for the safety assessment. This assumption is not suitable for wellhead jets. The method used is described below.

2.1. Well blowout dynamics

To evaluate the worst-case accident scenario, wellhead absolute open flow is commonly supposed to analyse sour gas well blowout [5,8]. Though detailed modeling of well-bore inflow is more proper to assess the surface release conditions, it is too complex to achieve and beyond the scope of this simulation. Whereas assuming the well bottom pressure is high enough so that the gas flow on the wellhead can reach choked condition, the initial condition for the wellhead mass flux is given by:

$$m_E = V_E \rho_E A \tag{2}$$

Based on Eq. (2), a balance between the mass flux, choked condition and casing or tubing inside diameter at well head can be achieved [8]. It is much easier to apply this method to do assessment, especially for a planned or under construction well, than to calculate the well-bore inflow which needs detailed information about the reservoir and casing program.

Then the release expands to atmospheric pressure and loses momentum due to changes in direction or impingement with the ground or structures without air entrainment. At the end of this process, the gas equation of state is applied as the pressure is equal to atmospheric pressure, and the well blowout is introduced to the

CFD model as velocity-inlet boundary defined by [8]:

$$V = \left(V_E + \frac{P_E - P_a}{\rho_E V_E}\right)\left(\frac{1 - C_D}{1 + C_D}\right) \tag{3}$$

Detailed calculation is based on ERCBH$_2$S, which accounts for real gas property and conservation of mass, momentum, and energy.

2.2. Combustion simulation

The mixture fraction-based combustion model is assumed for the ignition of sour gas, which is more simple and efficient in fire simulation compared with the finite-rate reaction [16]. As the calculation is done in large space, the reduction in computing resource and time is important.

The basic assumption is under a certain set of simplifications, the instantaneous thermochemical state of the fluid can be related to a conserved scalar quantity known as the mixture fraction f [17]. For every element involved in the combustion, f is defined as:

$$f = \frac{Z - Z_{ox}}{Z_{fuel} - Z_{ox}} \tag{4}$$

All the chemical reactions between sour gas (mostly methane, hydrogen sulfide and carbon dioxide) and atmosphere (mostly nitrogen and oxygen) are simplified into one single reaction without phase change:

$$CH_4 + 2H_2S + 5O_2 \rightarrow CO_2 + 4H_2O + 2SO_2$$

By introducing f, the chemistry is simplified into a mixture question, and the solving of nonlinear finite-rate chemistry is avoided. Under the assumption of chemical equilibrium, thermochemical scalars (species fractions, density, and temperature) are related to f. For a single mixture fraction, non-adiabatic system, the instantaneous values of thermochemical scalars are parameterized as:

$$\phi_i = \phi_i(f, H) \tag{5}$$

Regarding chemical nonequilibrium, the rich flammability limit (RFL) method of equilibrium chemistry model is used, in which fuel-rich regions are modeled as a mixed but unburnt mixture of pure fuel and a leaner equilibrium burnt mixture. The RFL of the fuel stream is estimated as 110–150% of the stoichiometric mixture fraction.

2.3. Gas dispersion model

Large eddy simulation (LES) associated with the mixture fraction transport equation is used as the theoretical basis for gas dispersion model, which is capable of simulating jet fire, reactive pollutant dispersion, and boundary flow in complex terrains. With fine grid resolution, a close agreement with experimental observations in jet fire simulation could be provided by LES [17]. Hu et al. studied the fire-induced buoyancy-driven plume in and above an idealized street canyon by using LES [12]. By comparing wind-tunnel observations with the predictions of various turbulence closure models, LES was shown to be capable of reproducing sensible results for flow over rough hills by Allen and Brown [18].

In LES, flow features that are larger than the grid size are resolved directly, whereas flow structures that are smaller than the grid size are modeled using a subgrid scale model. So a better balance between resource consumption and result accuracy is achieved compared with two other CFD turbulence models: direct numerical simulation (DNS) and Reynolds averaging Navier–Stokes equation (RANS). LES is more efficient in computation than DNS, and exhibits better agreement with the experimental results than RANS. Simulations of the neutrally stratified flow over Askervein Hill showed that LES provided an acceptable solution for the mean-velocity field and better predictions of the turbulent kinetic energy than RANS [11]. For transient mixing processes and the transient structure of turbulent fields, LES would be a better choice compared to RANS, as suggested by Li et al. [19]. The method used here is described below.

The equations for mass and momentum are as follows [17]:

$$\frac{\partial \overline{\rho}}{\partial t} + \frac{\partial}{\partial x_i}(\overline{\rho}\widetilde{u_i}) = 0 \tag{6}$$

$$\frac{\partial}{\partial t}(\overline{\rho}\widetilde{u_i}) + \frac{\partial}{\partial x_j}(\overline{\rho}\widetilde{u_i}\widetilde{u_j}) = -\frac{\partial \overline{p}}{\partial x_i} + \frac{\partial}{\partial x_j}\left[(\mu + \mu_t)\left(\frac{\partial \widetilde{u_i}}{\partial x_j} + \frac{\partial \widetilde{u_j}}{\partial x_i}\right)\right] + \overline{\rho} g_i \tag{7}$$

where μ_t is calculated by the Smagorinsky–Lilly model.

Under the assumption that the diffusivity of all species is equal and gas dispersion is dominated by turbulent convection, the species transport equations are replaced by a single mixture fraction equation:

$$\frac{\partial}{\partial t}(\overline{\rho}\overline{f}) + \frac{\partial}{\partial x_i}(\overline{\rho}\widetilde{u_i}\overline{f}) = \frac{\partial}{\partial x_i}\left(\frac{\mu_t}{\sigma_t}\frac{\partial \overline{f}}{\partial x_i}\right) + S \tag{8}$$

The turbulence–chemistry interactions are modeled by an assumed-shape probability density function approach [20]. For the relation between mean thermochemical scalars and their instantaneous values, assuming that the enthalpy fluctuations are independent of the enthalpy level, the equation is:

$$\overline{\phi_i} = \int_0^1 \phi_i(f, \overline{H}) p(f) df \tag{9}$$

where $p(f)$ is chosen as the double delta function, and is given by:

$$p(f) = \begin{cases} 0.5, & f = \overline{f} \pm \sqrt{\overline{f'^2}} \\ 0, & \text{elsewhere} \end{cases} \tag{10}$$

where $f' = f - \bar{f}$ and the mixture fraction variance is modeled in LES as:

$$\overline{f'^2} = C_v L_s^2 \left|\nabla \overline{f}\right|^2 \tag{11}$$

The transport equation for total enthalpy (sum of sensible and formation enthalpies) is:

$$\frac{\partial}{\partial t}(\overline{\rho}\overline{H}) + \frac{\partial}{\partial x_i}(\overline{\rho}\widetilde{u_i}\overline{H}) = \frac{\partial}{\partial x_i}\left(\frac{k_t}{c_p}\frac{\partial \overline{H}}{\partial x_i}\right) - S_{rad} + S_h \tag{12}$$

With the assumption of incompressible flow, the pressure work, kinetic energy, and viscous dissipation terms are not included [15]. The first term on the right-hand stands for the heat transfer due to conduction and species diffusion.

To fully account for the radiation, the radiative transfer equation should be solved which needs large computation [15]. As the hazard deriving from the radiation is not the concern in this study, a simple method is proposed to treat the heat loss due to radiation.

The total heat of combustion converted to radiation is calculated as:

$$Q_{rad} = \eta m_E H_c \tag{13}$$

where η is conversion factor for methane [21] which is the largest component of sour gas.

Then the S_{rad} is defined as:

$$S_{rad} = \frac{Q_{rad}}{V_f} \tag{14}$$

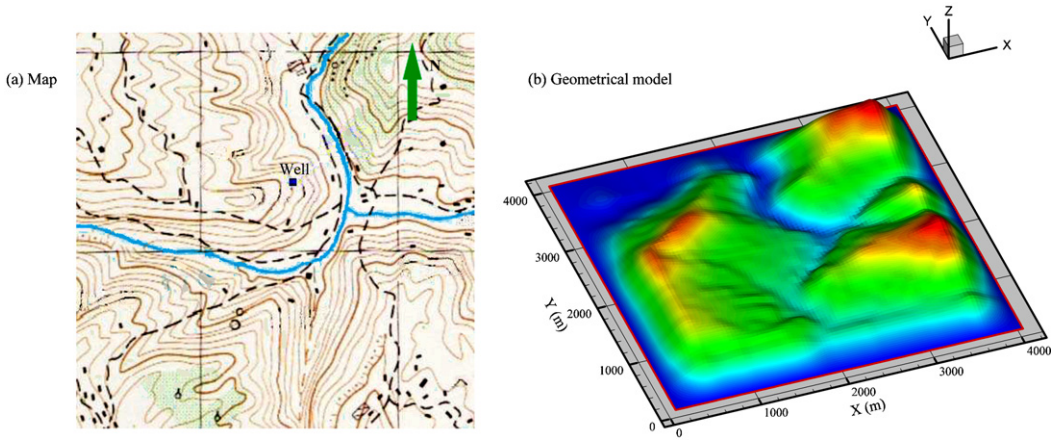

Fig. 1. The location of the example well. (a) Map, and (b) Geometrical model.

where V_f could be determined from [22]:

$$L_f = 0.00326(m_E H_c)^{0.478}$$
$$R_f = 0.29 s_f \left[\log_{10}\left(\frac{L_f}{s_f}\right)\right]^{0.5} \quad (15)$$

And it is added to the computational domain with the temperature higher than 773.15 K. The advantage of this method is that radiation is solved directly by means of energy absorption and no additional iterations are needed. Besides, the energy transferred to atmospheric environment is discounted so that the transport of product gas surrounding the flame is reduced to get a conservative estimate of the gas dispersion.

3. CFD calculation

3.1. Complex terrain modeling

A simple and practical method is proposed to reconstruct the terrains in the CFD geometrical model, which is based on SRTM 90-m digital elevation data for the entire world. First, natural relief is extended to a ramp zone around the boundaries. Next, spline interpolation is applied along each longitude and latitude to get continuous edges. Then, a four-sided surface standing for the real terrains is created from the two sets of parallel edges. This method is easy to be applied to other areas without the support of special software or tools, and the stiff curvature of reconstructed terrains is avoided by interpolation under the assumption of continuous terrains.

An example well from the Puguang highly sour gas field in the northeast of Sichuan and its geometrical model are showed in Fig. 1. The size of the computational domain is 3960 m × 3960 m × 1600 m, with the well set in the middle and north pointing at the +*Y*-axis. In the actual environment around the well, elevations increase toward the west and the maximum difference in altitude is about 300 m. In the east and south, the well is enclosed by a rivulet flowing from west to north. And from the lowest valley in the north to the well is about 180 m in elevation.

3.2. Dispersion conditions

Dispersion conditions have great influence on the consequences of accidents. In the atmospheric environment of low wind speed, temperature inversion, and stable atmosphere, the worst-case situation would be faced, caused by weak diffusion and sustained steady accumulation of SO_2. In order to reflect the atmospheric phenomena in the CFD model, the boundary layer flows are simulated by using the Pasquill atmospheric stability classes, and the corresponding profiles of wind speed and temperature along the altitude.

Class F is used to do conservative analysis. Then the empirical exponential law for wind speed profile is written as follows [23]:

$$\frac{v_1}{v_2} = \left(\frac{z_1}{z_2}\right)^{0.3} \quad (16)$$

For standard wind speed, according to environmental statistics on site, the mean wind speed is 1.0–1.8 m/s measured 10 m from the ground in all directions. The prevailing wind directions are calm winds, with the frequency of 37% and northeast 24% all year. The assessment is conducted with calm wind, and eight wind directions (E, NE, N, NW, W, SW, S and SE) with an annual average wind velocity of 1.3 m/s. The vertical temperature gradient is 4 K/100 m [23] and an annual average temperature of 289.95 K is used.

3.3. Numerical method

The three-dimensional computational domain is totally mapped with regular hexahedral elements after quadrilateral mesh generation for all boundaries and every part of the terrains. Vertical grid refinement is applied to side boundaries and core computational domain, and is shown in Fig. 2 on side plane and the slice.

In consideration of practical application, the domain is divided into 135 (X) × 138 (Y) × 116 (Z). The average grid spacing in the horizontal directions (X and Y) is between 12.5 and 100 m in the gas dispersion modeling over complex terrains of large scale [11,24,25]. The value we selected is 30 m. In the vertical direction (Z), the grid spacing from the ground to the top of the highest hill begins with a minimum size of 3 m stretched to a maximum size of 10 m. The grid-stretching ratio is 1.03. From the top of the highest hill to the up plane, the grid spacing is 10–60 m with the gird-stretching ratio of 1.04 [11].

All boundaries except wellhead are divided into five types as shown in Fig. 2, and the definitions are as follows: the inlet plane is set as a velocity-inlet boundary defined by vertical wind speed and temperature; the up plane is treated as a zero flux plane; the surface is defined as a no-slip wall, and wall function is also used to account for the inefficiency of grid resolution [26]; the others are outflow boundary.

An unsteady pressure-based solver is chosen to simulate an accidental scenario in two steps. First, simulation of the atmospheric flow is conducted without the wellhead jet; then, after a short time blowout, sour gas combustion and dispersion are calculated simultaneously. For every time step, the computing time requires about 5 min through parallel processing with Intel Quad-Core 2.83 GHz

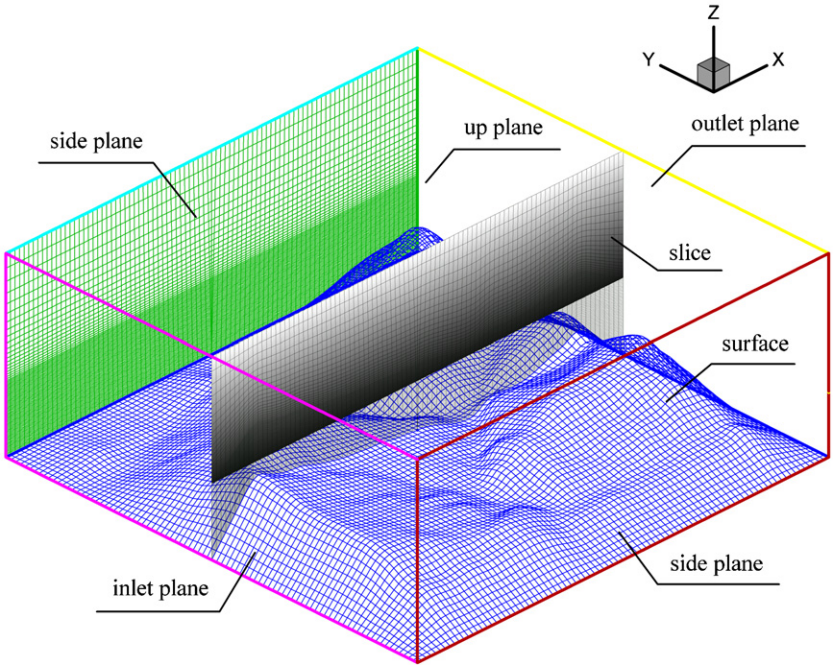

Fig. 2. Illustration of mesh and boundaries.

PC. With tests of various time steps, the distribution of the contaminated areas will change slightly with the time step of less than or equal to 1.5 s.

4. SO_2 poisoning assessment

Since that acute exposure to SO_2 is the main route of intoxication for the general public surrounding the well, the assessment is based on the dose–response relationship commonly used in acute toxicity research [21]. The toxic dose of potential exposure is evaluated by using the predicted concentration of SO_2 on the surface 146 cm above the ground. The height stands for the breathing zone, which is estimated by the average 136.7 cm shoulder height of standing Chinese adults [27] and a hemisphere of 15.24–22.86 cm diameter extending in front of the shoulder [28]. Considering that CFD results are discontinuous in time, linear interpolation of the concentration value is applied in integral intervals. The toxic dose is calculated as:

$$L = \int_0^{\tau_E} c^n d\tau = \sum_{k=0} \frac{1}{2}(c_k^n + c_{k+1}^n)\Delta\tau \tag{17}$$

Emergency response planning guideline (ERPG) levels developed by the American Industrial Hygiene Association are referenced as benchmarks for quantitative toxic environment assessment, which are based on acute toxicology data and designed to assist emergency response personnel planning for accidental chemical release to communities. For SO_2, the ERPG data are defined as exposure to airborne concentrations of 0.3, 3 and 15 parts per million (ppm) for up to 60 min [29]. For assessment facilitation, the equivalent ERPG concentration is used, which is associated with the estimated toxic dose through the following equation:

$$c_{eq} = \left(\frac{L}{60}\right)^{1/n} \tag{18}$$

n is chosen as 1.0 according to the Center for Chemical Process Safety [21], and the contaminated area is graded into low (0.3–3 ppm), moderate (3–15 ppm), and high hazard (≥15 ppm) regions.

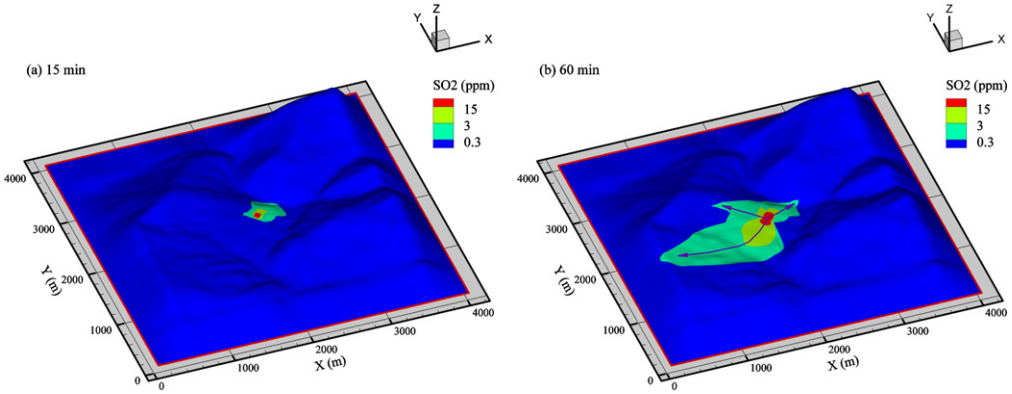

Fig. 3. The distribution of SO_2 hazard regions at different time after ignition at 1.3 m/s east wind. (a) 15 min, and (b) 60 min.

Table 1
Summaries of SO_2 contaminated areas.

Wind direction	Contaminated area (km^2)	Maximal influence distance (m)	Main trajectory
E	High: 0.028 Moderate: 0.19 Low: 1.05	High: SW 195 NE 83 Moderate: SW 620 NE 207 Low: SW 1684 NW 710 NE 535	(1) Northeast valleys (2) Northwest (3) Southwest
NE	High: 0.031 Moderate: 0.22 Low: 2.02	High: SW 184 Moderate: S 569 SW 501 Low: SW 1850 S 1,574	(1) South valleys (2) Downwind areas
N	High: 0.026 Moderate: 0.17 Low: 1.8	High: S 218 Moderate: S 568 Low: S 1935	(1) Downwind areas
NW	High: 0.072 Moderate: 0.36 Low: 2.47	High: SE 339 Moderate: SE 784 Low: SE 2023 S 1850	(1) South valleys (2) Downwind areas
W	High: 0.030 Moderate: 0.13 Low: 0.89	High: NE 190 Moderate: NE 420 Low: E 1550 NE 807	(1) Northeast valleys (2) Downwind areas
SW	High: 0.048 Moderate: 0.30 Low: 3.40	High: NE 318 Moderate: NE 675 Low: NE 1995	(1) Downwind areas
S	High: 0.036 Moderate: 0.18 Low: 2.49	High: N 230 Moderate: NW 725 N 562 Low: N 2033 NW 1897	(1) Northeast (2) Downwind areas
SE	High: 0.067 Moderate: 0.48 Low: 2.95	High: NW 340 Moderate: NW 947 Low: NW 2362	(1) Downwind areas
C	High: 0.013 Moderate: 0.032 Low: 1.28	High: R 80 Moderate: N 264 Low: N 1690	(1) Vicinities of the well (2) North valleys

5. Result and discussion

The basic information about the example well is 2.5×10^4 m^3/h of wellhead absolute open volume flux, 15.16% of volume fraction of hydrogen sulfide, and 5 min of ignition delay time.

5.1. Analysis of SO_2 contaminated areas

An illustration of the results with east winds is shown in Fig. 3. With high energy deriving from combustion and under the effects of wind, SO_2 disperses quickly and impacts a wide area that is irregular in shape. Within 15 min after ignition, the projection areas of high, moderate, and low hazard regions are 0.0051, 0.012, and 0.15 km^2, respectively. After 60 min, these regions increase to 0.028, 0.19, and 1.05 km^2 in area, respectively.

In Fig. 3(a), the contaminated area is mainly distributed in the NE. A high hazard region surrounds the well with a maximal radius of 64 m. Moderate and low hazard regions head in a NE direction, with the farthest distances of 168 and 446 m, respectively. In Fig. 3(b), the contaminated area is mainly distributed in the SW and NW. High and moderate hazard regions extend to distances of 195 and 620 m in the SW, respectively. The maximal influence distances of low hazard regions are 1684 and 710 m in the SW and NW, respectively. In addition, the influence distances of high, moderate, and low hazard regions increase to 83, 207, and 535 m in the NE, respectively.

So the dispersion process could be estimated as: at an early stage, the plume accumulates in the valleys in the NE; then, the hazard regions spread downwind in SW and NW directions. The main trajectories of SO_2 include northeast valleys, and the northwest and southwest around the hills, which are indicated by arrows in Fig. 3(b).

The quantitative statistics of assessment results at different wind directions 60 min after ignition are shown in Table 1.

5.2. Influence of wind and terrain

As the effects on SO_2 dispersion produced by wind are influenced by terrain and vice versa, conjoint analysis is carried out here.

In Fig. 4, the contaminated area of narrow ellipse is generated by east winds up to 5 m/s, quite different from Fig. 3(a). The hazard regions cover a much wider area under high wind speed. High, moderate, and low hazard regions are 0.0071, 0.013, and 0.35 km^2 in area, respectively, with corresponding maximal influence distances of 144, 294, and 1,705 m. The growth compared with the values in Fig. 3(a) is shown in Fig. 5. However, the impact is reduced. The average and maximal equivalent ERPG concentrations are 6.01 ppm versus 11.31 ppm and 239.43 ppm versus

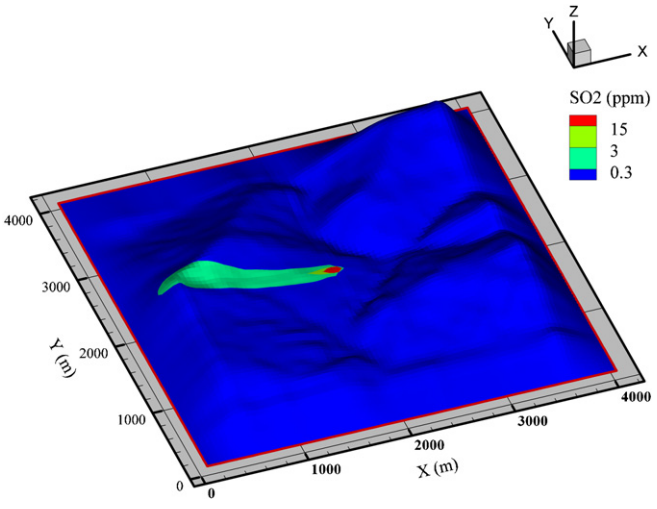

Fig. 4. The distribution of SO_2 hazard regions at 5 m/s east wind after 15 min.

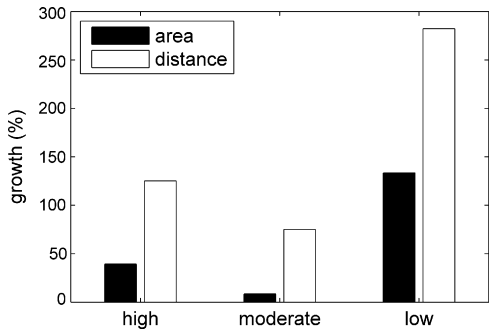

Fig. 5. The growth of hazard area and distance at higher wind speed.

339.81 ppm. In addition, these regions head straight west without obviously distributing in the upwind area. In this situation, the transportation of SO_2 by wind is primary, which drives the gas plume to cross the hills and suppress the gravity sedimentation of SO_2.

Comparing Fig. 6 to Fig. 3(b), significant differences exist in the distribution of the contaminated area, which are mainly caused by different terrain patterns. On the one hand, favorable terrain patterns such as valleys and basins, where wind speed is reduced and wind direction swirls, facilitate the sedimentation of SO_2. In Fig. 6, the winding valleys in the east are the largest part of the hazard regions. Though these areas are in the upwind direction in Fig. 3(b), the hazard exists there too, which is something to which attention should be paid. On the other hand, the plume is blocked and forced to change directions by the raised areas of the terrain. In Fig. 6, the downwind movement of SO_2 is restricted by a small hill in the east, which is in favor of the extension of hazard regions in the piedmont valleys. In Fig. 3(b), the plume direction turns to the southwest, where the terrains are relatively flat compared with those of the west.

In summary, wind drives the hazard regions to spread downwind, which is the dominant factor for the distribution of hazard regions and could inhibit the effects of the terrains with the increase of wind speed. In addition, the shape of the hazard regions is changed by terrains under the effects of spatial aggregation and obstacles. However, the effects are hard to determine due to various characteristics of terrains and nonuniform distributions.

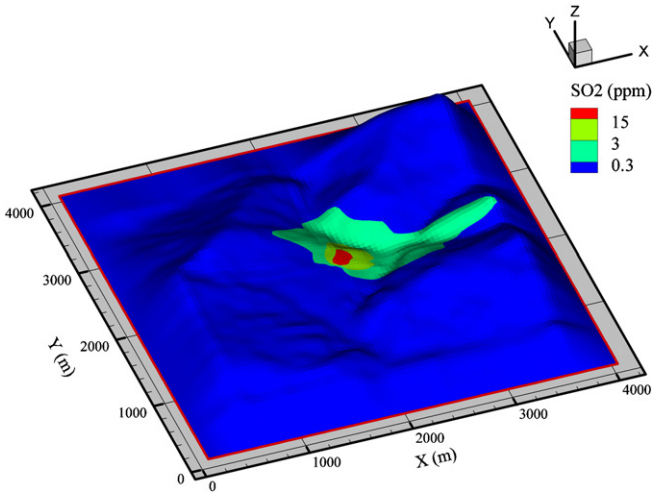

Fig. 6. The distribution of SO_2 hazard regions at 1.3 m/s west wind after 60 min.

5.3. Distribution features of the contaminated area

Under the interactions of wind and terrain, the hazard regions always spread in downwind areas, the front of the slopes, and depression areas such as valleys. However, without specific analysis, the appropriate estimation of the distribution is hard to make. In contrast to the situation in flat terrains, the hazard regions extend in several directions except for the downwind direction. The potential trajectories probably appear in the depression areas around the source and vicinities along the downwind direction where the terrains are flatter compared to the surrounding area.

Generally, worst-case dispersion conditions typically defined by low wind speed and stable atmospheric turbulence are chosen to do risk assessment. The hypothesis is that the affected regions predicted using this method could cover the largest potential accidental zone. However, the distribution of the contaminated area is so different from each other in complex terrains that a wide range of dispersion conditions should be included in addition to the worst-case scenario for practical applications such as emergency response planning.

5.4. Influence on emergency response

According to the analysis of distribution features of the contaminated area, terrain patterns conducive to gas dispersion and accumulation also facilitate human activities in the hills. Most people live in level ground suitable for building and agriculture. Roads and railways are always built through mountain passes, along riversides, and around mountainsides. These increase the possibility that the general public will be exposed to SO_2 in case of an accident.

During the emergency response, evacuation of the general public and transportation of huge amounts of emergency resources, such as equipment, and rescuers will be necessary. In view of the transportation system in the hills, the traffic load may increase to a level beyond the transport capacity. For example, there is only one road near the example well along the rivulet from west to north, with the capacity of one heavy vehicle. Considering that the rescue vehicles are mostly trucks, cranes, ambulances, and the like, and have to travel from the emergency response center located to the west of the well, the possibility of traffic congestion is quite high. As a result, the accident will be exacerbated by rescue delay and the evacuated are exposed to toxic gas for additional time due to a slow evacuation.

It can be concluded that the dispersed toxic gas is a great disadvantage to emergency response in relation to population distribution and transportation capacity in complex terrains, and the bottleneck restriction comes from the transportation capacity.

5.5. Effectiveness in controlling the number of deaths

Though the effectiveness in controlling the number of deaths by ignition of uncontrolled sour gas from well blowout is verified by the practical application [4], it is still valuable to provide another support for decision making in theory. Based on estimated toxic dose, probit for SO_2 lethal toxicity can be calculated according to [21]:

$$Y = -15.67 + \ln L \tag{19}$$

In association with Eq. (18), the minimum lethal equivalent ERPG concentration is about 1.06×10^5 ppm. Calculation is done for all nine wind directions with combustion duration of 60 min. The results are all lower than that, meaning the theoretical probability of death is zero, which is quite in accordance with accident investigation.

6. Conclusions

To study the SO_2 poisoning due to ignition of uncontrolled sour gas flow of well blowout in hills, an integrated model is proposed to simulate the accident process of wellhead jet, sour gas combustion, and products dispersion, and to evaluate the consequences of SO_2 poisoning. The effective quantitative results provided by the simulations are useful for safety applications such as risk assessment and emergency response planning.

In complex terrains such as hills, the potential accidental consequences are varied with uncertain factors, mainly coming from the interactions of wind and terrain. As a result, the SO_2 will impact a wide area of an irregular shape in multiple directions during an accident. Considering that the real-time prediction of the toxic gas dispersion in complex terrains and atmospheric environment is still hard to obtain with current computer speeds, a well-prepared assessment of the potential hazard regions will be valuable to accident rescue. At least, preliminary accident analysis under the worst-case and most occurrences of dispersion conditions in eight wind directions should be performed.

In order to prevent the potential damage to the general public from the SO_2, a well-designed public protection plan should be added to the existing standards and guidelines in China, in which the related information is not so well specified. The adoptable measures include public notification, evacuation, and sheltering, which could be referred to Directive 071 issued by ERCB [3]. For the oil and gas companies and local governments, the emergency plan is deserved to pay attention to the traffic management to achieve a safe, timely, and orderly transportation of emergency resources and evacuation of the general public. To overcome the adverse effects of transportation capacity, it is suggested that temporary area monitors and portable shelters are provided along the main evacuation roads to help people take refuge and reduce the exposure to toxic gas.

It has been proven that SO_2 cannot cause death in practice and theory. So ignition decision should be made by on-site executive without hesitation under extreme conditions.

Acknowledgement

This research is supported by the National Key Science and Technology Programs of China for large oil and gas field exploitation (Project No: 2008ZX05017).

References

[1] Technical Committee of Safety Standardization for Oil Industry, SY/T 5087-2005 Recommended practice for safe drilling operations involving hydrogen sulfide, National Development and Reform Commission, Beijing, China, 2005.
[2] SINOPEC Office of Science and Technology, Q/SH 0033-2007 Safety technique specification of gas well drilling and downhole operation in the Northeast of Sichuan, China Petrochemical Corporation, Beijing, China, 2007.
[3] ERCB, Directive 071 Emergency preparedness and response requirements for the petroleum industry, ERCB, Calgary, Canada, 2008.
[4] Jianfeng Li, Bin Zhang, Yang Wang, Mao Liu, The unfolding of '12.23' Kaixian blowout accident in China, Saf. Sci. 47 (2009) 1107–1117.
[5] Kaiji Zhou, Xin1 Liu, Zhaoxue Guo, Qiji Yuan, Lei Zhou, Study on the method predicting spurt speed of uncontrolled blowout at wellhead, Nat. Gas Ind. 26 (2006) 71–73.
[6] Chen Jianguo, Pan Siming, Lu Yi, Yuan Hongyong, Numerical prediction and transportation study of poisonous gas transport on complex terrain, J. Tsinghua Univ. (Sci. Technol.) 47 (2007) 1–4.
[7] Jianfeng Li, Bin Zhang, Mao Liu, Yang Wang, Numerical simulation of the large-scale malignant environment pollution incident, Process Saf. Environ. (2009) 232–244, Prot. 87.
[8] ERCB, ERCBH2S A Model for Calculating Emergency Response and Planning Zones for Sour Gas Facilities. Volume 1: Technical Reference Document, ERCB, Calgary, Canada, 2008.
[9] P.A. Taylor, H.W. Teunissen, The Askervein hill project: overview and background data, Bound. -Layer Meteorol. 39 (1987) 15–39.
[10] M. Btruer, N. Peller, Ch. Rapp, M. Manhart, Flow over periodic hills—numerical and experimental study in a wide range of Reynolds numbers, Comput. Fluids 38 (2009) 433–457.
[11] A. Silva Lopes, J.M.L.M. Palma, F.A. Castro, Simulation of the Askervein flow. Part 2: Large-eddy simulations, Bound. -Layer Meteorol. 125 (2007) 85–108.
[12] L.H. Hu, R. Huo, D. Yang, Large eddy simulation of fire-induced buoyancy driven plume dispersion in an urban street canyon under perpendicular wind flow, J. Hazard. Mater. 166 (2009) 394–406.
[13] Paola Blotto, Michele Bonuccelli, Gianni Morale, Edoardo Dellarole, Mariano Falcitelli, Fabrizio Podenzani, Development of a integrated approach to the risk analysis of a blow-out accident, SPE 86704.
[14] Lorenzo Borello, Michele Bonuccelli, Gianni Morale, The CFD approach for the risk analysis of a blowout event, SPE 108619.
[15] FLUENT Inc. FLUENT 6.3 Help Document.
[16] Kevin Mcgrattan, Bryan Klein, Simo Hostikka, Jason Floyd, Fire Dynamics Simulator (Version 5) User's Guide, NIST, Washington, DC, USA, 2008.
[17] S.L. Brennan, D.V. Makarov, V. Molkov, LES of high pressure hydrogen jet fire, J. Loss Prev. Process Ind. 22 (2009) 353–359.
[18] T. Allen, A.R. Brown, Large-eddy simulation of turbulent separated flow over rough hills, Bound. -Layer Meteorol. 102 (2002) 177–198.
[19] Xian-Xiang Li, Chun-Ho Liu, Dennis Y.C. Leung, K.M. Lam, Recent progress in CFD modeling of wind field and pollutant transport in street canyons, Atmos. Environ. 40 (2006) 5640–5658.
[20] A. Khelil, H. Naji, L. Loukarfi, G. Mompean, Prediction of a high swirled natural gas diffusion flume using a PDF model, Fuel 88 (2009) 374–381.
[21] Center for Chemical Process Safety of the American Institute of Chemical Engineers, Guidelines for Consequence Analysis of Chemical Releases, American Institute of Chemical Engineers, New York, USA, 1999, pp. 216–261.
[22] Sam Mannan, Lee's Loss Prevention in the Process Industries. Volume 1: Hazard Identification, Assessment and Control, 3rd ed., Elsevier Butterworth-Heinemann Publications, Burlington, USA, 2005, pp. 16/220.
[23] European Process Safety Centre, Atmospheric Dispersion, Institution of Chemical Engineers (IChemE), Rugby, UK, 1999, pp. 17–31.
[24] K. Hanjalic, S. Kenjeres, Dynamic simulation of pollutant dispersion over complex urban terrains: a tool for sustainable development, control and management, Energy 30 (2005) 1481–1497.
[25] F. Scargiali, E. Di Rienzo, M. Ciofalo, F. Grisafi, A. Brucato, Heavy gas dispersion modelling over a topographically complex mesoscale a CFD based approach, Process Saf. Environ. Prot. 83 (2005) 242–256.
[26] Bert Blocken, Ted Stathopoulos, Jan Carmeliet, CFD simulation of the atmospheric boundary layer: wall function problems, Atmos. Environ. 41 (2007) 238–252.
[27] China National Institute of Standardization and Information Classification and Coding, GB 10000-1988 Human dimensions of Chinese adults, National Bureau of Quality and Technical Supervision, Beijing, China, 1988.
[28] Technical Committee of Safety Standardization for Oil Industry, SY/T 6137-2005 Recommended practices for oil and gas producing and gas processing plant operations involving hydrogen sulfide, National Development and Reform Commission, Beijing, China, 2005.
[29] Emergency Response Planning (ERP) and Workplace Environmental Exposure Level (WEEL) Committees, AIHA 2008 Emergency Response Planning Guidelines (ERPG) & Workplace Environmental Exposure Levels (WEEL) Handbook, American Industrial Hygiene Association, Fairfax, USA, 2008, pp. 1–27.